

INORGANIC CHEMISTRY

FRONTIERS

Accepted Manuscript



This article can be cited before page numbers have been issued, to do this please use: I. Basma, K. Rediger, C. Kasahara, H. Abul-Futouh, M. Micheel, M. K. Farh, P. Köhler, G. Mlosto, M. Wächtler and W. Weigand, *Inorg. Chem. Front.*, 2025, DOI: 10.1039/D5QI01191D.



This is an Accepted Manuscript, which has been through the Royal Society of Chemistry peer review process and has been accepted for publication.

Accepted Manuscripts are published online shortly after acceptance, before technical editing, formatting and proof reading. Using this free service, authors can make their results available to the community, in citable form, before we publish the edited article. We will replace this Accepted Manuscript with the edited and formatted Advance Article as soon as it is available.

You can find more information about Accepted Manuscripts in the [Information for Authors](#).

Please note that technical editing may introduce minor changes to the text and/or graphics, which may alter content. The journal's standard [Terms & Conditions](#) and the [Ethical guidelines](#) still apply. In no event shall the Royal Society of Chemistry be held responsible for any errors or omissions in this Accepted Manuscript or any consequences arising from the use of any information it contains.

Engineered [FeFe]-Hydrogenase Mimics Featuring Heteroaryl Linkers: Molecular Design and Photocatalytic Hydrogen Evolution Under Visible Light

Ibrahim Basma^{†a}, Katharina Rediger^{†b}, Chizuru Kasahara^a, Hassan Abul-Futouh^{*c}, Mathias Micheel^{‡b}, Micheal K. Farh^{◇d}, Phil Köhler^a, Grzegorz Mlostoń^e, Maria Wächtler^{§*b} and Wolfgang Weigand^{*a}

^a Institute for Inorganic and Analytical Chemistry, Friedrich Schiller University Jena, Humboldtstr. 8, 07743 Jena, Germany. Email: wolfgang.weigand@uni-jena.de.

^b Department of Chemistry and State Research Center OPTIMAS, RPTU Kaiserslautern-Landau, Erwin-Schrödinger-Str. 52, 67663 Kaiserslautern, Germany.

^c Department of Chemistry, Faculty of Science, The Hashemite University, P.O. Box 330127, Zarqa 13133, Jordan. Email: h.abulfutouh@hu.edu.jo.

^d Department of Chemistry, Faculty of Science, Assiut University, 71515 Assiut, Egypt.

^e Department of Organic & Applied Chemistry, University of Łódź, Tamka 12, 91-403 Łódź, Poland.

[‡] Current address: Institute for Technical Chemistry and Environmental Chemistry, Friedrich-Schiller University Jena, Philosophenweg 7a, 07743 Jena, Germany.

[◇] Current address: Center for Energy and Environmental Chemistry Jena (CEEC Jena), Friedrich Schiller University Jena, Philosophenweg 7a, 07743 Jena, Germany.

[§] Current address: Institute of Physical Chemistry and Kiel Nano, Surface and Interface Science (KiNSIS), Kiel University, Max-Eyth-Str. 1, 24118 Kiel, Germany. Email: waechtler@phc.uni-kiel.de.



Abstract

Inspired by the active site of [FeFe]-hydrogenase, we have developed synthetic mimics engineered from the reaction of heteroaryl thioketone derivatives ferrocenyl(5-(4-(diphenylamino)phenyl)thiophen-2-yl)methanethione (**PS-Fc-1**), ferrocenyl(5'-(4-(diphenylamino)phenyl)-[2,2'-bithiophen]-5-yl)methanethione (**PS-Fc-2**) and phenyl(5'-(4-(diphenylamino)phenyl)-[2,2'-bithiophen]-5-yl)methanethione (**PS-Ph**) as pro-ligands with $\text{Fe}_3(\text{CO})_{12}$. The resulting complexes contain thiolato ligands which enable a close linkage between heteroaryl chromophores and the catalytic center, thereby promoting efficient photocatalytic hydrogen evolution under visible light irradiation. These mimics incorporate a push-pull organic chromophore, consisting of triphenylamine and (bi)thiophene groups, designed to facilitate direct photoexcitation into a charge-separated state. Electrochemical properties were examined using cyclic voltammetry, and photophysical characteristics were determined by steady-state spectroscopy and nanosecond transient absorption supported by (TD-)DFT simulations. Whilst both catalytically active species revealed the formation of charge-separated states, directly upon excitation, fast deactivation due to relaxation into low-lying ferrocene-located states prevents the formation of long-living excited states in the ferrocene-linked dyad. This explains the reduced activity for hydrogen generation of the dyad containing the ferrocene moiety compared to phenyl one.



Introduction

Energy is considered the keystone for productivity improvement in agriculture and industrial sectors. However, the main energy source for most of the world's energy requirements is governed by fossil fuels, which are the primary driver of greenhouse gas emissions. Therefore, the search for eco-friendly alternatives to reduce these emissions is progressively becoming a major concern of industrial developers and world governments.¹⁻³ It is important to consider that any alternative selected should be abundant, affordable, environmentally sustainable, and widely available across regions to effectively compete with traditional fuels. Among the sustainable energy sources, green hydrogen is considered the most viable long-term solution that meets these criteria. Green hydrogen can be produced via photocatalysis using visible sunlight as the sole energy.^{4,5} A photocatalytic system is typically achieved through the combination of a catalyst (CAT) and a photosensitizer (PS), with the support of a sacrificial electron donor (SED), to ensure the thermodynamic feasibility of catalytic reactions while inhibiting unproductive back-electron transfer. In the interest of economic and environmental impact, the most efficient photocatalytic system should be one in which both the CAT and the PS are designed entirely of earth-abundant elements and provide long-term stability and high ability for hydrogen formation.^{6,7} Such photocatalytic systems can be either intermolecular, in which the photoactive unit is separated from the catalyst, or intramolecular where the photoactive unit is combined with the catalytic center as a single entity.⁸ The former is considered less efficient as it is limited by diffusion processes bringing the PS and the CAT close enough to facilitate the transfer of electrons from the excited PS to the CAT center.^{8,9-11} A paradigm for a catalyst based on earth abundant elements is provided by nature. The protein [FeFe]-hydrogenase is recognized as a highly efficient catalyst for hydrogen formation, with a reported turnover frequency (TOF) greater than 10^4 s^{-1} under optimal conditions.^{12,13} The structure of the active site (so-called H-cluster) of [FeFe]-hydrogenase revealed by X-ray crystallographic analysis is represented in Figure 1.¹⁴⁻¹⁷ As shown in Figure 1, the topology of the H-cluster contains a butterfly [2Fe2S] subunit acting as the catalyst center for proton reduction and an [4Fe4S] ferredoxin cluster that is responsible for the electron transfer to the H-cluster.¹⁴ Inspired by the natural archetype of [FeFe]-hydrogenase, a variety of its mimics have been developed to function as catalysts for the electrochemical reduction of



protons.¹⁸⁻²⁵ Building on this existing knowledge, it is instinctive to explore the potential applications of these mimics as catalysts also in photochemical hydrogen production processes. In this context, photochemically driven proton reduction systems have been achieved through the combination of PS and an [FeFe]-hydrogenase mimic as a CAT.²⁶⁻³¹

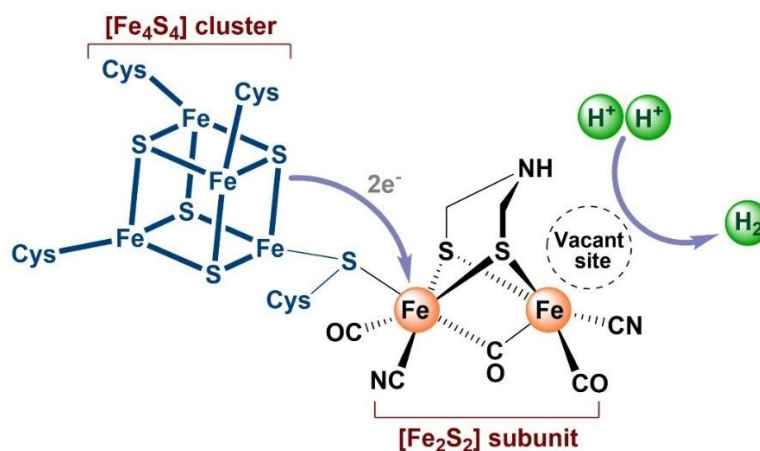


Figure 1. The active site of natural [FeFe]-hydrogenase.

Reviewing the literature of these photochemically driven proton reduction systems, one can find that the PS can be bonded to the CAT in two different strategies, both with concomitant advantages and disadvantages.³¹ In the first strategy, the PS is attached to the CAT via the organic dithiolato linker, while the second approach relies on introducing the PS directly to one of the iron centers through a ligand as an alternative to one of the terminal CO groups.^{28,32-41} Following the first scenario, the group of Sun reported the first example of this strategy in which acetylene-functionalized ruthenium bis(terpyridine) complex was selected as the PS, and the synthetic model of [FeFe]-hydrogenase, $[\text{Fe}_2(\text{CO})_6\{\mu-(\text{SCH}_2)_2\text{NR}\}]$ ($\text{R} = \text{C}_6\text{H}_5\text{I}$), was used as the CAT.³² As a result, the spectroscopic and electrochemical data of their dyad system indicate that oxidative quenching of the photoexcited $^*[\text{Ru}(\text{terpy})_2]^{2+}$ by the CAT was uphill by 0.59 eV.⁴² In subsequent years, further studies on such a system using dyads containing Ru- or Re-based photosensitizers or organic chromophores have been reported and they showed a diversity in their turnover number (TON) for light-driven hydrogen evolution.³¹ However, the highest TON of 31.8 was observed in a study by Hou and co-workers, in which they synthesized a dyad system by covalently connecting two metal-free PSs and one $[\text{Fe}_2\text{S}_2]$ cluster.⁴³ The ongoing



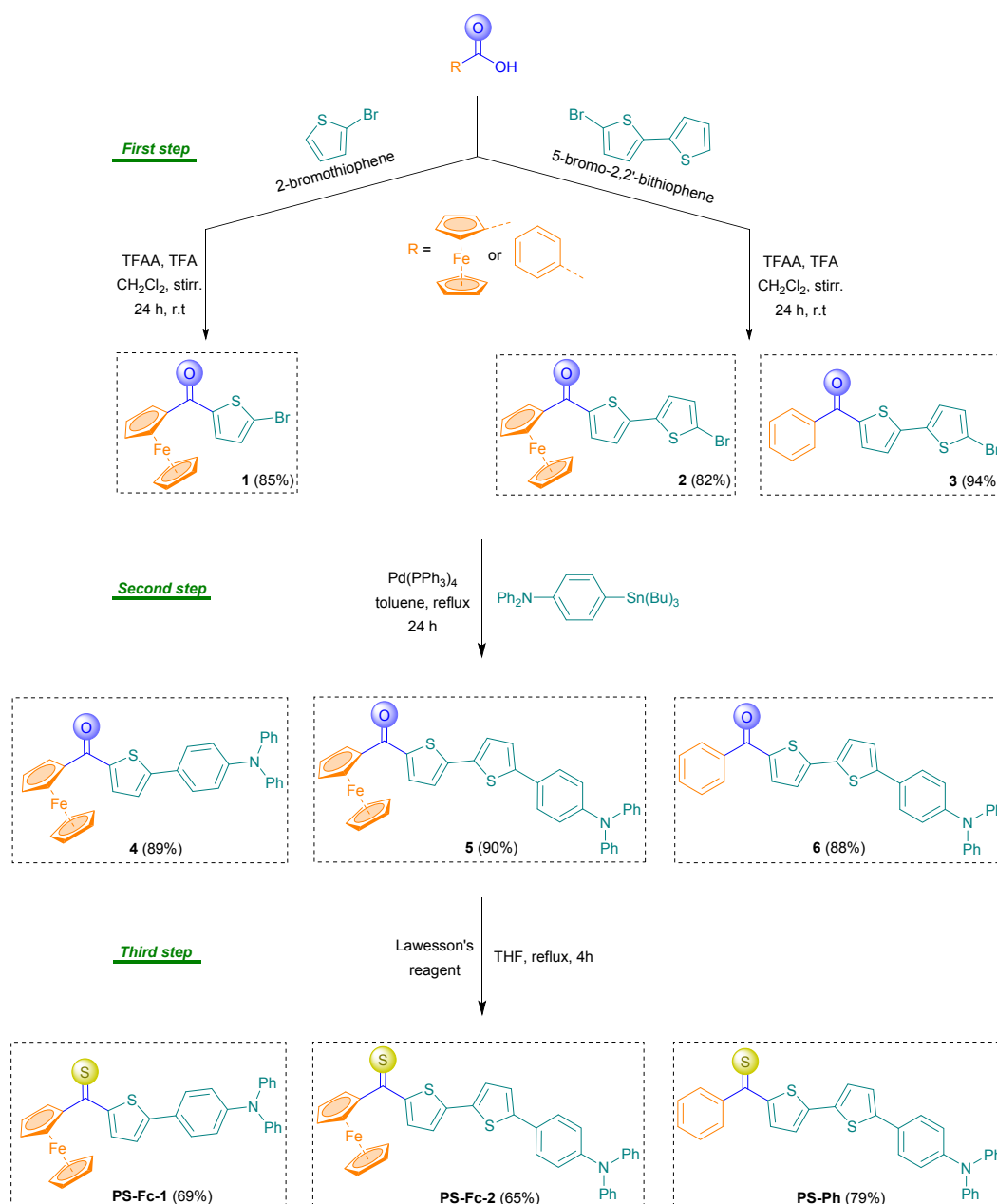
development of these scenarios has led our group to design a new class of dyads that absorbs light in the UV region. This includes a small, compact, heavy-metal-free, photosensitizer-catalyst dyad by utilizing a silicon-containing heteroaromatic system.^{44,45} In this study, a TON of 539 was reached after 7 hours of irradiation under optimal conditions, and hence it is considered the highest reported value at that time for such small compact systems. More recently, we have designed another prototype dyad comprising π -conjugated oligothiophenes as light absorbers, which shows a remarkable long-term photocatalytic activity among the reported analogous complexes in the visible spectral range.⁴⁶ Considering these remarkable findings and our ongoing interest in the reaction of heteroaryl thioketones with $\text{Fe}_3(\text{CO})_{12}$, we aimed to design photoactive thioketone derivatives that are good at absorbing visible light.^{24,47,48} These derivatives can react with $\text{Fe}_3(\text{CO})_{12}$ to form [FeFe]-hydrogenase mimicking complexes that can be activated by visible light. The thioketones developed in this study are composed of three essential components: i) the thiocarbonyl group, ii) a ferrocenyl moiety, and iii) a push-pull organic chromophore based on triphenylamine and (bi)thiophene aimed at direct photoexcitation into a charge-separated state. The thiocarbonyl group is regarded as the reactive site for coordination with the metal center and the good donor ability of the ferrocenyl group is expected to enhance the electron density in such a system, supporting the reactivity for the coupling and increasing stability. Further, the ferrocenyl moiety could act as intrinsic electron donor, and hence support the formation of charge-separated state and charge carrier accumulation at the FeFe center.⁴⁹⁻⁵³ The resulting [FeFe]-hydrogenase mimicking complexes are investigated for their abilities for photocatalytic hydrogen generation under visible light. Additionally, to evaluate the impact of the ferrocenyl moiety, which can act as an electron donor but also as energy acceptor, a structural analogue featuring a phenyl ring in place of the ferrocenyl group has been synthesized.⁵⁴ Moreover, the known compound 4-([2,2'-bithiophen]-5-yl)-*N,N*-diphenylaniline (**PS**) has been synthesized for comparison, following the method previously reported in the literature.⁵⁵

Results and discussion

Synthesis and characterization



The synthetic routes of obtaining the target systems are outlined in Scheme 1. Initially, the reaction of ferrocenecarboxylic acid with 2-bromothiophene or 5-bromo-2,2'-bithiophene in CH_2Cl_2 solution produced compounds **1** and **2**, respectively, as shown in Scheme 1 (first step).



Scheme 1. Preparation of compounds **1–6** and **PS-Fc-1**, **PS-Fc-2**, and **PS-Ph**. First step: Friedel-Crafts acylation. Second step: Stille coupling. Third step: thionation using Lawesson's.



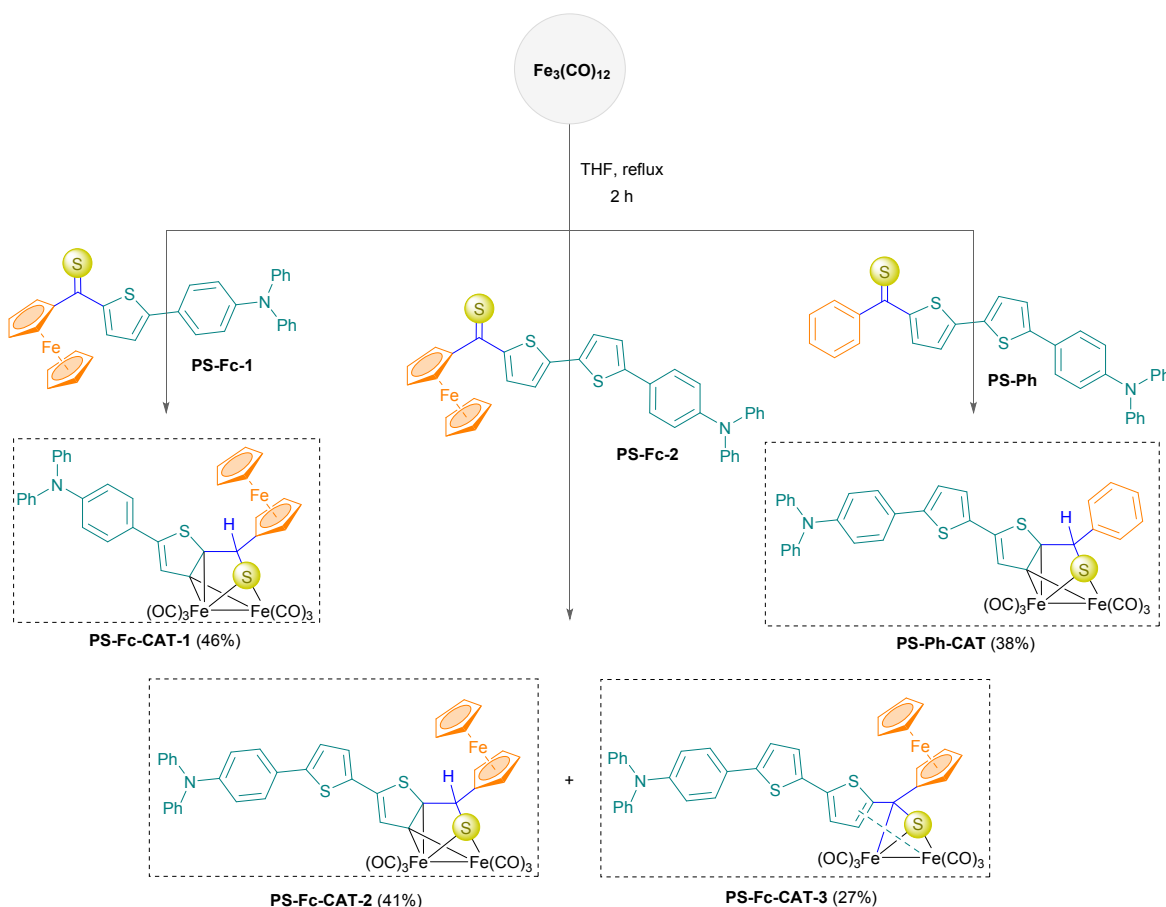
In parallel, the reaction of benzoic acid with 5-bromo-2,2'-bithiophene under the same conditions afforded compound **3** (Scheme 1, first step). In the subsequent step, compounds **1–3** were reacted with *N,N*-diphenyl-4-(tributylstannyl)aniline, respectively, in the presence of Pd(PPh₃)₄ as a catalyst, resulting in the formation of the desired compounds **4–6**, respectively, as depicted in Scheme 1 (second step). Compounds **1–6** have been characterized by means of ¹H, and ¹³C{¹H} NMR spectroscopic techniques as well as elemental analysis, mass spectrometry and single-crystal X-ray structure determination of compound **4** (Figure S1, ESI), which are described in detail in the ESI part. The next step involved thionating the carbonyl groups in compounds **4–6** using Lawesson's reagent in THF at 65 °C for 4 hours, resulting in compounds **PS-Fc-1**, **PS-Fc-2**, and **PS-Ph** with moderate yields as shown in Scheme 1 (third step). The obtained compounds were characterized by spectroscopic techniques (¹H and ¹³C{¹H} NMR, Figures S14-S19, ESI), IR (Figures S41-43, ESI), mass spectrometry (Figures S31-33, ESI), and elemental analysis. The absence of signals corresponding to the ketone group in the ¹³C{¹H} NMR spectra of compounds **PS-Fc-1**, **PS-Fc-2**, and **PS-Ph** along with the appearance of a signal around 220 ppm for the carbon atoms of the thioketone group confirmed the postulated structures of these compounds.

Synthesis and characterization of diiron complexes

Treatment of equimolar amounts of Fe₃(CO)₁₂ and compounds **PS-Fc-1**, **PS-Fc-2**, and **PS-Ph** in boiling THF for 2 hours, followed by column chromatography, afforded complexes **PS-Fc-CAT-1**, **PS-Fc-CAT-2**, **PS-Fc-CAT-3**, and **PS-Ph-CAT** with isolated yields ranging from 27% to 46% as depicted in Scheme 2. Notably, only compound **PS-Fc-2** produced a mixture of *ortho*-metalated complexes **PS-Fc-CAT-2** and **PS-Fc-CAT-3** under similar conditions (Scheme 2). This behavior has been previously observed in similar reaction of thioketone derivatives with Fe₃(CO)₁₂, as reported by our group.^{30,47} The new complexes were characterized by ¹H and ¹³C{¹H} NMR, IR, UV-Vis spectroscopy, mass spectrometry, elemental analysis, cyclic voltammetry, and X-ray crystallography for complex **PS-Fc-CAT-2**.



The IR spectra of complexes **PS-Fc-CAT-1**, **PS-Fc-CAT-2**, and **PS-Ph-CAT** (Figures S44, 45, 47, ESI) reveal three absorption bands located at 2068, 2027, 1987 cm^{-1} (for **PS-Fc-CAT-1**); 2068, 2029, 1990 cm^{-1} (for **PS-Fc-CAT-2**); and 2070, 2031, 1994 cm^{-1} (for **PS-Ph-CAT**), corresponding to the terminal CO ligands. In contrast, the IR spectrum of complex **PS-Fc-CAT-3** (Figure S46, ESI) shows four characteristic metal/carbonyl stretching bands located at 2043, 2035, 2000, and 1946 cm^{-1} . The obtained results are consistent with those of the corresponding iron complexes reported in the literature.^{30,47} It is noteworthy that the frequencies of complex **PS-Ph-CAT** are slightly shifted to higher values compared to those of complexes **PS-Fc-CAT-1** and **PS-Fc-CAT-2**, indicating a weaker electron-donating character of the phenyl ring to the FeFe center compared to the ferrocene one.



Scheme 2. Synthetic routes of complexes **PS-Fc-CAT-1-3** and **PS-Ph-CAT**.



The ^1H NMR spectra of complexes **PS-Fc-CAT-1**, **PS-Fc-CAT-2**, and **PS-Ph-CAT** (Figures S20, 22, 26, ESI) display a singlet resonance that is related to the methine moieties in the region of 5.40–5.57 ppm. However, this resonance is completely absent in the spectrum of **PS-Fc-CAT-3** (Figure S24, ESI), indicative of a distinct alteration in its structure. Moreover, nine protons of the ferrocene moiety in complexes **PS-Fc-CAT-1-3** were also detected in the area between 3.21 and 4.74 ppm. The signals of the other protons, which confirmed the proposed structures of the obtained complexes, were also detected within the expected range. The $^{13}\text{C}\{^1\text{H}\}$ NMR spectrum of **PS-Fc-CAT-3** (Figure S25, ESI) display a distinct singlet resonance at approximately 179.0 ppm, which is absent in the spectra of **PS-Fc-CAT-1**, **PS-Fc-CAT-2**, and **PS-Ph-CAT** (Figures S21, 23, 27, ESI). This resonance is attributed to the carbon atom adjacent to the ferrocene moiety and hence providing strong support for the proposed structure of **PS-Fc-CAT-3**. Additionally, all complexes show signals of the terminal carbonyl carbon atoms of the iron cores in the range of 209.0–213.0 ppm (Figures S21, 23, 25, 27, ESI).

The molecular structure of complex **PS-Fc-CAT-2** was unambiguously determined through single crystal X-ray diffraction, and its molecular geometry is depicted in Figure 2. A suitable single crystal of complex **PS-Fc-CAT-2** was successfully gained through the diffusion of pentane into a CH_2Cl_2 solution of complex **PS-Fc-CAT-2** at a low temperature ($-20\text{ }^\circ\text{C}$). It is evident from Figure 2 that the thiolato ligand in complex **PS-Fc-CAT-2** is bound to the two iron centers via the sulfur atom, with an average Fe–S bond length of 2.2552(7) Å, which is consistent with those of its analogous reported in the literature.^{30,47}



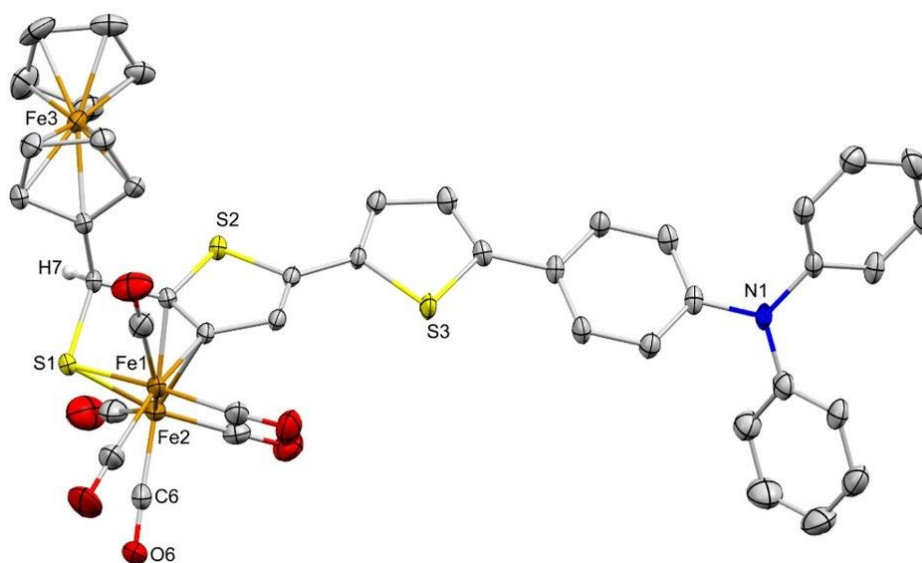


Figure 2. Molecular structure of compound **PS-Fc-CAT-2** in the crystal. Displacement ellipsoids are drawn at the 50% probability level, H-atoms omitted for clarity.

Moreover, complex **PS-Fc-CAT-2** features a σ -bond to one iron atom (Fe1) through the β -carbon of the thiophene ring, directly bonded to the thiolato moiety, while the other iron atom (Fe2) is π -coordinated to the α - and β -C atoms of the same thiophene ring in a η^2 -mode. The Fe–Fe bond length in complex **PS-Fc-CAT-2** (2.5311(6) Å) is comparable to those of similar complexes described in the literature.^{30,47} The average Fe–CO bond length in complex **PS-Fc-CAT-2** (1.7937(3) Å) aligns with those observed for analogous complexes reported in the literature.^{30,47} The ferrocene moiety in complex **PS-Fc-CAT-2** adopts an eclipsed conformation.

The electrochemical behavior of the resulting complexes was investigated by applying cyclic voltammetry in CH_2Cl_2 -[*n*Bu₄N][BF₄] solution at a scan rate of 0.2 V/s (V referenced to the Fc⁺/Fc couple).



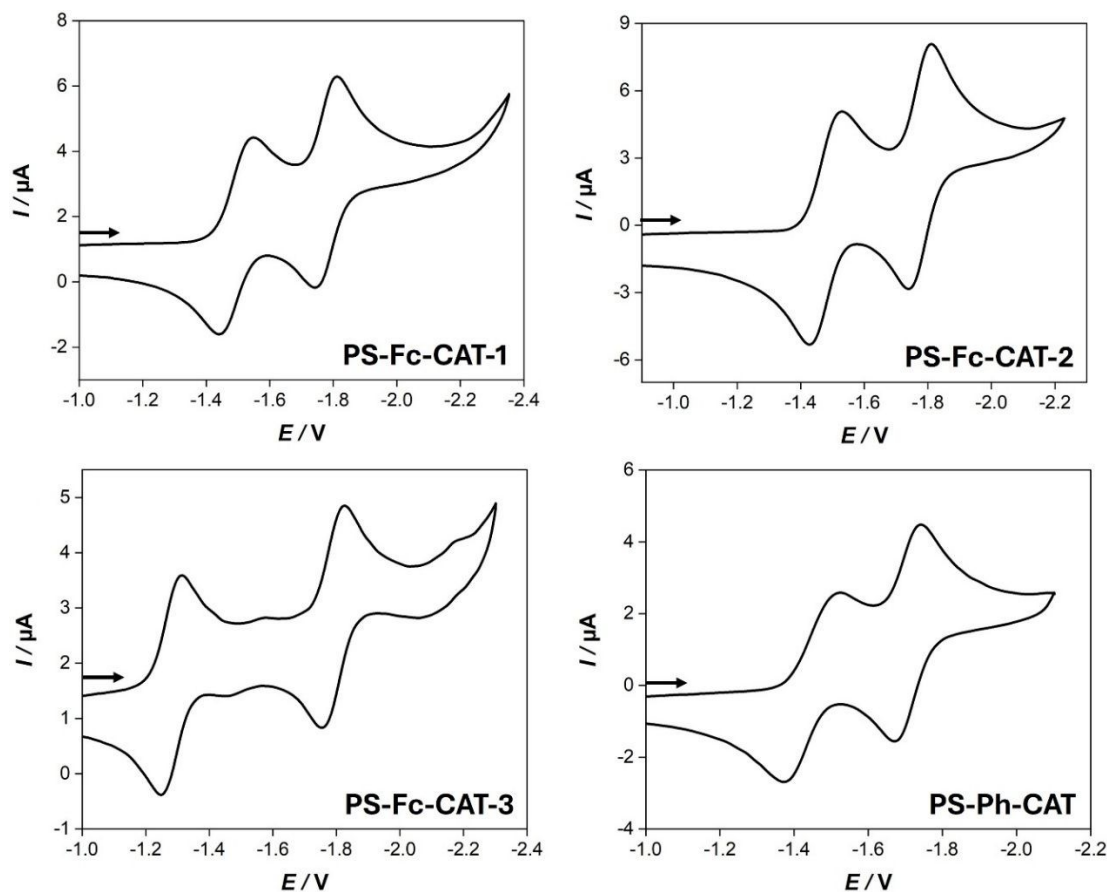


Figure 3. Cyclic voltammetry of 1.0 mM of complexes **PS-Fc-CAT-1-3** and **PS-Ph-CAT** in CH_2Cl_2 -[$n\text{Bu}_4\text{N}$][BF_4] (0.1 M) solutions at 0.2 V/s scan rate using glassy carbon disk ($d = 1.6$ mm). The arrows indicate the scan direction. The potentials E are given in V and referenced to the Fc^+/Fc couple.

As indicated in Figure 3, the cyclic voltammogram of each complex exhibited two reversible couples in the reduction region at $E_{1/2} = -1.49$ and -1.78 V (for **PS-Fc-CAT-1**), $E_{1/2} = -1.48$ and -1.77 V (for **PS-Fc-CAT-2**), $E_{1/2} = -1.28$ and -1.79 V (for **PS-Fc-CAT-3**), as well as $E_{1/2} = -1.45$ and -1.71 V (for **PS-Ph-CAT**). These two reversible couples can be assigned to the $\text{Fe}^{\text{I}}\text{-Fe}^{\text{I}} \rightarrow \text{Fe}^{\text{I}}\text{-Fe}^0$ couple and $\text{Fe}^{\text{I}}\text{-Fe}^0 \rightarrow \text{Fe}^0\text{-Fe}^0$ couple, respectively. This behavior is similar to that of its analog reported in the literature, and the reduction values of these complexes are shifted to lower values compared to those of the analog.³⁰



Photocatalytic activities

The photocatalytic H₂ production activities of molecular dyad (**PS-CAT** without Fc) as well as molecular triad (**PS-CAT** with Fc) were investigated under visible light irradiation. Initially, in order to determine the excitation wavelength of **PS-CATs**, the UV-vis absorption of complexes was recorded in CH₂Cl₂. **PS-Fc-CAT-2**, **PS-Fc-CAT-3**, and **PS-Ph-CAT** (Figure S48, ESI) showed strong absorption bands around 393, 651, and 390 nm, respectively. Contrarily, complex **PS-Fc-CAT-1** only absorbs radiation in the UV region (Figure S48, ESI) in accordance with the size of the conjugated system of the chromophoric oligothiophene unit. Accordingly, **PS-Fc-CAT-2**, **PS-Fc-CAT-3**, and **PS-Ph-CAT** were tested for their hydrogen evolution activity. For this purpose, photocatalysis under visible light irradiation in the presence of BIH (1,3-dimethyl-2-phenylbenzimidazoline) as both electron and proton source were performed. **PS-Fc-CAT-2** and **PS-Ph-CAT** showed catalytic activity under 405 nm irradiation. In contrast, **PS-Fc-CAT-3** was inactive for hydrogen evolution, under 625 nm irradiation which agrees with observations recently reported for a related system with a diene linker between the sensitizer and the catalyst unit.⁴⁷ Figure 4 shows the time profile of the H₂ evolution of **PS-Fc-CAT-2** and **PS-Ph-CAT**. The turnover numbers (TON) after 20 h of irradiation reached ~294 and ~112 for **PS-Ph-CAT** and **PS-Fc-CAT-2**, respectively. It is noteworthy that the turnover frequencies (TOF) for the initial 2 hours of irradiation were ~55.4 h⁻¹ for the dyad and ~2.6 h⁻¹ for the triad. However, the triad showed superior stability of the catalysis, i.e., **PS-Ph-CAT** lost its catalytic activity after 12 hours of irradiation, though **PS-Fc-CAT** kept producing H₂ beyond this period. The findings indicated that the Fc provided catalytic stability; however, it exerted a negative influence on the catalytic efficiency of the triad. Nevertheless, compared to our previously reported [FeFe]-hydrogenase mimics with visible activity, the TOF of **PS-Ph-CAT** was significantly higher.^{46,47} This phenomenon suggests that the thioketone structure provides **PS-CAT** with unique photoexcited properties. In order to gain insights into the photoexcited states of dyads and triads, and the underlying reasons for their efficiency and stability, nanosecond transient absorption (ns-TA) of **PS-Ph-CAT** and **PS-Fc-CAT-2** was performed.



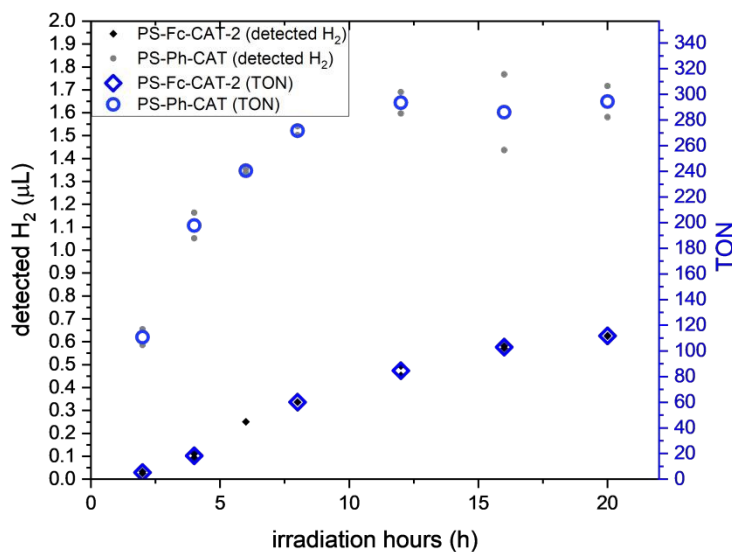


Figure 4. Time profile of photocatalytic H₂ production and TON of **PS-Fc-CAT-2** and **PS-Ph-CAT**. The catalyst concentrations were 10 μM, and the BIH concentrations were 10 mM in the acetonitrile/*N*-methyl-2-pyrrolidone = 1/3 mixture under 405 nm irradiation

Properties of excited states in PS-CAT dyads

To explore the manifold of excited states and analyze the excitation conditions, the absorption spectra of the dyads **PS-Ph-CAT** and **PS-Fc-CAT-2** are compared to a model sensitizer **PS**. Upon linking the catalysts to the sensitizer **PS**, slight characteristic changes in the absorption and emission properties are observed (Figure 5). The absorption spectrum of the sensitizer unit **PS** shows two absorption features at 305 nm ($\epsilon = 4.4 \cdot 10^4 \text{ Lmol}^{-1}\text{cm}^{-1}$) and 379 nm ($\epsilon = 8.3 \cdot 10^4 \text{ Lmol}^{-1}\text{cm}^{-1}$) and a broad, intense emission band at 459 nm, which is independent of the excitation wavelength (Figure S51, ESI). The absorption spectra and, thus the electronic structure of the modified sensitizer species **PS-Fc-2** and **PS-Ph** acting as precursors for the dyads, were revealed to be heavily influenced by the additionally introduced thioketone functionality. Although changes in the photophysical properties due to the linkage of either the phenyl or ferrocenyl groups are evident in the absorption spectra, the absorption features of the dyads are more comparable to the unsubstituted sensitizer **PS**. Hence, once the reaction center is linked to the sensitizers to form **PS-Fc-CAT-2** and **PS-Ph-CAT** the absorption spectra more closely resemble **PS** than the thioketone form of the sensitizers. The catalyst **PS-Ph-CAT** reveals a split UV absorption feature with peaks



at 283 nm ($\epsilon = 2.9 \cdot 10^4 \text{ L mol}^{-1} \text{ cm}^{-1}$) and 301 nm ($\epsilon = 2.8 \cdot 10^4 \text{ L mol}^{-1} \text{ cm}^{-1}$) and a peak at 390 nm ($\epsilon = 2.8 \cdot 10^4 \text{ L mol}^{-1} \text{ cm}^{-1}$) in the UV region. Additionally, a pronounced shoulder in the visible absorption region develops at 482 nm ($\epsilon = 1.0 \cdot 10^4 \text{ L mol}^{-1} \text{ cm}^{-1}$). The absorption spectrum of the ferrocene-containing catalyst **PS-Fc-CAT-2** exhibits two strong bands at 303 nm ($\epsilon = 3.1 \cdot 10^4 \text{ L mol}^{-1} \text{ cm}^{-1}$) and 393 nm ($\epsilon = 3.8 \cdot 10^4 \text{ L mol}^{-1} \text{ cm}^{-1}$) with the latter one, similar to **PS-Ph-CAT** extending into a shoulder up to 600 nm. The emission intensity is strongly quenched in both dyads and both systems show only a weak emission band with a peak at around 490 nm and a second strongly redshifted broad feature (Figure S51, ESI). This indicates that the presence of the catalyst is quenching the emitting state and the residual emission in the dyad is further reduced by the presence of the ferrocene unit.

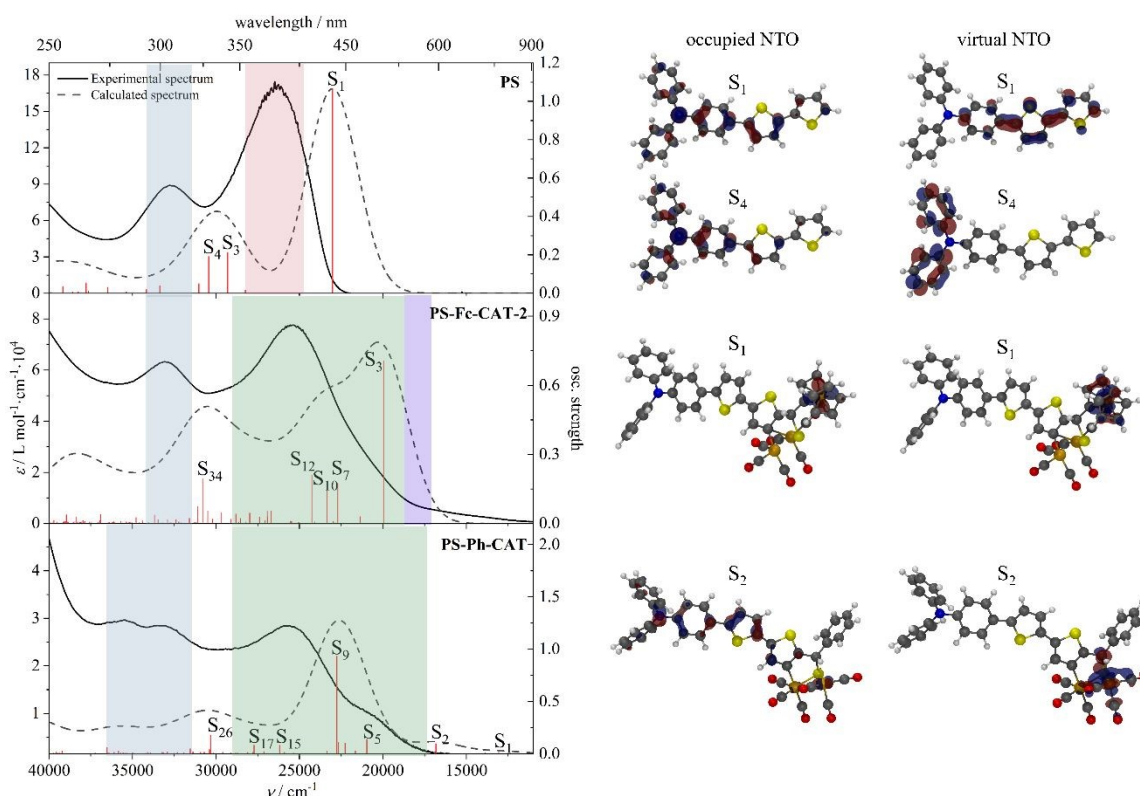


Figure 5. Experimental (solid line) and calculated (dashed line) UV-vis spectra of **PS** (top), **PS-Fc-CAT-2** (middle), and **PS-Ph-CAT** (bottom) with the calculated vertical transition energies and oscillator strengths indicated as red bars. Regions assigned to transitions isolated at certain functional groups are highlighted with grey, push-pull transitions from the triphenylamine unit to the thiophene with red, ferrocenyl-centered transitions with violet, and charge-transfer (CT) transition from the sensitizer to the [FeFe]-center with



green. The most important transitions of each spectrum are represented as NTO (natural transition orbital) on the right.

To explore the character of the electronic states responsible for light absorption TD-DFT calculations (for details on the theoretical methods and calculations, see ESI) were performed (Figure 5). The calculated UV-vis absorption spectrum of **PS** allows to assign the strong absorption feature at 379 nm in the experimental spectrum of **PS** to a strongly dipole-allowed transition to the S_1 state ($f = 1.08$) which mainly contains contributions of the HOMO to LUMO transition with $^1\pi\pi^*$ character. Excitation to the S_1 state leads to a decreased electron density at the amine nitrogen atom and a subsequent increase at the thiophene units and thus shows slight push-pull character induced by the electron-rich triphenylamine unit, although **PS** does not contain a strong acceptor group.^{56,57} The weaker absorption band at 305 nm is represented by the calculated transitions to the S_3 and S_4 state ($f = 0.22$ and $f = 0.19$ respectively) with contributions of both the thiophene and triphenylamine unit in the initial as well as the final state with $^1\pi\pi^*$ character. In the dyad and triad, the character of these short wavelength transitions remains basically unchanged, while the push-pull transition appears red-shifted compared to **PS** in accordance with the red-shift in the experimental absorption spectra and shows increased push-pull character with the catalyst unit acting as acceptor. Hence, in the dyad and triad, these transitions possess direct charge-transfer character from the sensitizer unit to the catalyst (Figure 5). However, the most prominent differences in the **PS-Ph-CAT** and **PS-Fc-CAT-2** electronic transitions can be found in the energetically low-lying shoulders in the visible range of the absorption spectra. In the ferrocenyl linked triad, **PS-Fc-CAT-2**, the extension of this shoulder can be assigned to the two energetically lowest weak transitions S_1 and S_2 at 550 nm ($f = 1.00 \cdot 10^{-4}$ and $f = 2.55 \cdot 10^{-5}$ respectively). Both transitions are exclusively located at the ferrocene moiety being isolated from the [FeFe]-center and the sensitizing unit. The low oscillator strength of the energetically lower excited states S_1 and S_2 is in line with the observed decreased emission intensity compared to **PS** and also evident in the emission spectra of ferrocenyl-linked sensitizer species **PS-Fc-2**. Compared to the phenyl-linked dyad **PS-Ph-CAT** the transitions S_1 and S_2 ($f = 0.03$ and $f = 0.10$ respectively) are located at the [FeFe]-center with contributions of the sensitizer unit indicating some shifting of electron density from the light-harvesting unit to the catalytically active center.



Additionally, transition S_5 ($f = 0.14$) also assigned to the shoulder in the visible range of **PS-Ph-CATs** experimental absorption spectrum is of push-pull character with the [FeFe]-center as electron density acceptor and the light-harvesting sensitizer unit acting as donor. Also, the triad **PS-Fc-CAT-2** facilitates these push-pull transitions resembled by excitation into the S_3 , S_{10} and S_{12} state ($f = 0.71$, $f = 0.14$ and $f = 0.21$ respectively).

As a result, such strong optically allowed transitions with push-pull nature could be a source of efficient charge separation and thus high catalytic activity. Besides the presence of transitions with strong direct charge transfer, additional [FeFe]-centered low lying states are present and could be a possible deactivation pathway. Further, the ferrocenyl-linked triad revealed the lowest states to be ferrocene-centered, which could be source of additional deactivation of photocatalytically active excited states via relaxation of these states by energy transfer to the Fc unit.⁵⁸⁻⁶¹ This hypothesis is in line with the observed strong quenching of the singlet excited state in the ferrocene-linked compounds and the slightly quenched emission in the [FeFe]-linked dyads.

Previous studies in thiophene-based hydrogenase mimics indicate long-lived triplet states of oligothiophenes to play a crucial role in the activation mechanism leading to catalytic activity.^{46,62} To elucidate whether in the newly developed dyads this is also the case, nanosecond transient absorption spectroscopy was performed to probe the via intersystem crossing formed triplet in oligothiophene chromophores. As expected, the sensitizer **PS** exhibits broad excited state absorption (ESA) with an absorption maximum at 600 nm (Figure 6). The transient absorption signal decays mono-exponentially with a lifetime of $\tau = 29.0 \pm 0.13$ μ s. This feature can be assigned to the thiophene located $^3\pi\pi^*$ state also in good agreement with TD-DFT calculations (Figure S53, ESI) and to previous results reported in literature.^{46,62} Unfortunately, due to the instability of **PS-Ph-CAT** under the conditions of the ns-TA measurements, the excited state lifetime could only be estimated from a measurement at a single probe wavelength at 600 nm (Figure 6). At 600 nm potentially residual signal from $^3\pi\pi^*$ sensitizer-centered excited state as observed for **PS** can be detected with a lifetime estimated to be 38.3 ± 2.27 μ s. Nevertheless, the influence of photo products caused by degradation of the dyad cannot be excluded. For the triad **PS-Fc-CAT-2**, which is stable under the measurement conditions, no long-lived sensitizer



triplet state can be detected at all (Figure 6). These findings for **PS-Ph-CAT** and **PS** indicate together with the strong quenching of the singlet state emission in both species, that probably the formation of a **PS**-localized $^3\pi\pi^*$ triplet state is not taking place in this case and that a fast alternative channel already occurring from the singlet state is active in these systems. This could be related to the changed character of the excited singlet states, changing the character of the visible absorption from a $\pi\pi^*$ to a charge transfer state, directly inducing charge separation between the sensitizer and the catalyst. Further, the presence [FeFe]-centered low lying states opens the possibility population of these states, opening a general loss channel. In **PS-Fc-CAT-2** additionally the population and formally excitation energy transfer to the Fc unit is increasing this effect.⁶³ All four processes can be the source of absence of any long-lived triplet signature either preventing the formation of the triplet in the first place or quickly quenching this state. The process transferring excitation to the Fc unit only present in **PS-Fc-CAT-2** could be responsible for the decreased activity compared to **PS-Ph-CAT**. This interpretation is supported by the location of the spin density of the lowest excited triplet state being centered at the catalytically active [FeFe]-center in the **PS-Ph-CAT** dyad (Figure S70, ESI) but being located at the inactive ferrocene (Figure S74, ESI) in the **PS-CAT-Fc-2** species. Also, measurements in the presence of electron donor BIH were conducted and delivered no sign of any long-lived species for the **PS-Fc-CAT-2** species with a reduced $[\text{Fe}^0\text{Fe}^I]$ -center. This indicates that both charge-separated state and doublet states ESA of **PS-Fc-CAT-2** are taking place on time scales below the measurement range potentially further influenced by the proton donating ability of BIH forming protonated intermediates.

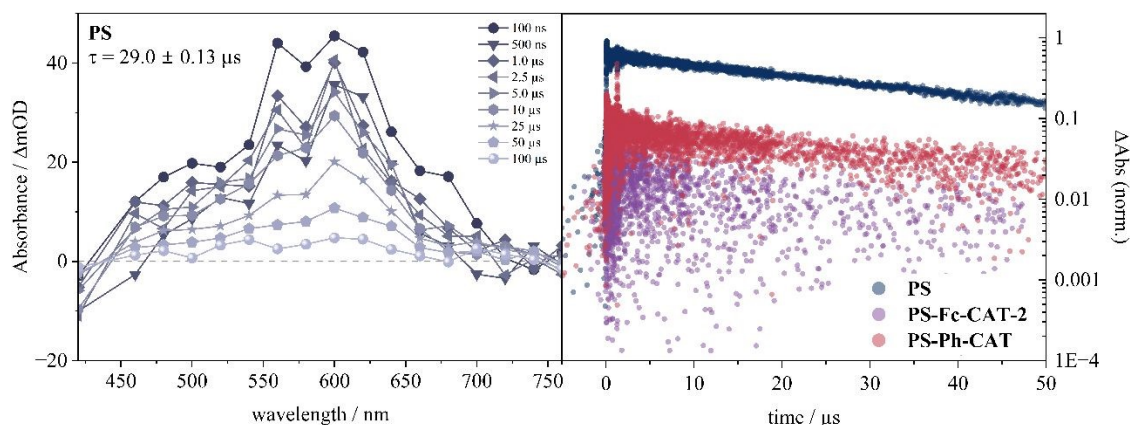


Figure 6. Nanosecond transient absorption spectra of 21 μM **PS** solution in CH_2Cl_2 at different time delays (left) and kinetic decays at 600 nm of 21 μM **PS**, 27 μM **PS-Fc-CAT-2** and 20 μM **PS-Ph-CAT** normalized by the absorbance of **PS** at $\lambda_{\text{exc}} = 440$ nm (right).

Activation, reduction and hydrogen evolution pathway of PS-Ph-CAT and PS-Fc-CAT-2

In the light of the data presented, we are suggesting the following mechanism explaining the activity of the system. The results from the analysis of the singlet excited state manifold indicate a drastic change in character of the visible absorption features revealing a unique charge density shifting transition of CT character with the triphenylamine group acting as electron rich donor unit and the [FeFe]-hydrogenase mimic as acceptor. This results in **PS-Ph-CAT** to a direct charge-separation already upon excitation transferring electron density towards the catalyst. This could be the reason for the observed increased catalytic activity compared to previously reported systems, where $\pi\pi^*$ excitation of the sensitizers thiophene unit is followed by ISC and charge transfer occurring from the triplet state manifold is a necessary step. This process is bypassed in the reported systems via a direct push-pull transition which transfers charge carriers from the sensitizer to the catalyst directly. This is in agreement with the observation of a strong quenching of the emission from the singlet sensitizer state. Nevertheless, the singlet excited charge transfer state is not the lowest state in the system and [FeFe]-centered states are also present and could be a source of radiationless deactivation. If the population of such state could be prevented a further increase in catalytic activity is expected to occur. The ferrocene unit in **PS-Fc-CAT-2** causes a further quenching of emission and additionally reduces the catalytic activity compared to **PS-Ph-CAT**. This indicates a significant interference of the ferrocene unit. There are two known pathways for the quenching mechanism, one including an energy transfer step and a second one with electron transfer from the donor ferrocene to an acceptor.^{46,62} Energy transfer to the ferrocene and subsequent thermal relaxation populates a catalytic inactive state, while ferrocene acting as electron donor would be expected to activate the system either via reductive quenching the **PS** unit in **PS-Fc-CAT-2** and supporting subsequent electron transfer to the catalyst from the reduced sensitizer, or in the case of direct charge transfer as observed in our system preventing recombination by



reduction of the formally oxidized **PS**.⁶¹ The decreased activity for hydrogen evolution of the Fc containing triad suggests the energy transfer pathway to be active and though the triad **PS-Fc-CAT-2** shows increased stability the activity for hydrogen evolution is decreased.

Conclusion

In summary, we have developed a series of new photoactive thioketones, **PS-Fc-1**, **PS-Fc-2**, and **PS-Ph**, which react with $\text{Fe}_3(\text{CO})_{12}$ to form [FeFe]-hydrogenase mimicking complexes, namely **PS-Fc-CAT-1**, **PS-Fc-CAT-2**, **PS-Fc-CAT-3**, and **PS-Ph-CAT**. These complexes were thoroughly characterized using various analytical techniques, including ^1H and $^{13}\text{C}\{^1\text{H}\}$ NMR, IR spectroscopy, mass spectrometry, and elemental analysis, with X-ray crystallographic analysis performed on **PS-Fc-CAT-2**. By integrating a thiocarbonyl group, a ferrocenyl or phenyl moiety, and a push-pull organic chromophore, these systems are strategically engineered for direct photoexcitation into a charge-separated state. Furthermore, their potential for photocatalytic hydrogen evolution under visible light irradiation was explored. Among the synthesized complexes, only **PS-Fc-CAT-2** and **PS-Ph-CAT** exhibited catalytic activity under 405 nm irradiation. Further, the ferrocenyl-linked dyad revealed a decreased activity compared to **PS-Ph-CAT** indicating a deactivating rather than activating influence of the ferrocene. This is in line with the observed quenched emission and absent ns TA signal upon linkage of the ferrocene to the dyad, which is due to low lying Fc-centered excited states causing fast deactivation of the catalyst. However, the incorporation of the ferrocenyl unit can be justified by its ability to enhance the overall stability of the system, thereby contributing to the development of a more durable catalyst for future applications. In contrast, the increased catalytic activity of **PS-Ph-CAT** can be explained by population of a charge transfer state transferring electron density from the sensitizer to the catalyst directly upon light excitation.

The presented work once more demonstrates the practical usefulness of ferrocenyl thioketones for synthesis of diverse ferrocenyl functionalized compounds which are of importance for preparation of medically relevant compounds, e.g. ferrocifenes as well as for materials chemistry.⁶⁴⁻⁶⁸

Experimental part



Materials and techniques

All manipulations concerning the preparation of all complexes were performed using standard Schlenk and vacuum-line techniques under an inert gas (Ar). The ^1H and $^{13}\text{C}\{^1\text{H}\}$ NMR spectra were recorded with a Bruker Avance 400 or 600 MHz spectrometer. Chemical shifts are given in parts per million with references to internal SiMe_4 (^1H , $^{13}\text{C}\{^1\text{H}\}$). The mass spectrum was recorded with Finnigan MAT SSQ 710 instrument. Elemental analysis was performed with a Leco CHNS-932 apparatus. TLC was performed by using Merck TLC aluminum sheets (Silica gel 60 F254). Solvents from Fisher Scientific and other chemicals from Across and Aldrich were used without further purification. All solvents were dried and distilled prior to use according to standard methods. Compound **PS** was synthesized according to the procedure reported in the literature.⁵⁵ The synthetic procedures and characterization of compounds **1-6** are described in detail in the supplementary part.

Electrochemistry:

Corrections for the iR drop were performed for all experiments. CV measurements were conducted in three electrode technique [glassy carbon disk (diameter=1.6 mm) as working electrode, Ag/Ag^+ in MeCN as reference electrode, Pt wire as counter electrode] using a Reference 600 Potentiostat (Gamry Instruments). All experiments were performed in CH_2Cl_2 solutions (concentration of the complexes 1.0 mM) containing 0.1 M $[\text{nBu}_4\text{N}][\text{BF}_4]$ at room temperature. The solutions were purged with N_2 and a stream of it was maintained over the solutions during the measurements. The vitreous carbon disk was polished on a felt tissue with alumina before each measurement. All potential values reported in this paper are referenced to the potential of the ferrocenium/ferrocene (Fc^+/Fc) couple.

Crystal structure determination

The single-crystal X-ray intensity data for the reported compounds were collected on a Bruker-Nonius Kappa-CCD diffractometer equipped with a Mo-K α I μ S microfocus source and an Apex2 CCD detector, at $T = 120(2)$ K. The crystal structures were solved with SHELXT-2018/3 and refined by full matrix least-squares methods on F^2 with SHELXL-



2018/3, using the Olex2 1.3 environment.⁶⁹⁻⁷¹ Multi-scan absorption correction was applied to the intensity data.⁷² Restraints on the interatomic distances and anisotropic displacement parameters were used for the disordered C₄S ring in compound **4** (SADI and SIMU commands in ShelXL).⁷⁰ CCDC 2445996 (for **PS-Fc-CAT-2**) and 2445997 (for **4**) contain the supplementary crystallographic data for this paper (see Table S1). These data can be obtained free of charge from The Cambridge Crystallographic Data Centre (CCDC; <http://www.ccdc.cam.ac.uk>).

Steady-state spectroscopy

UV-vis absorption spectroscopy was carried out with a SPECORD S600 (Analytik Jena) and a Lambda 900 double-beam spectrometer (Perkin Elmer). Emission spectroscopy was performed with a Fluorolog 3-22 τ Spectrometer (Horiba Jobin Yvon).

Nanosecond transient absorption spectroscopy

The time-resolved transient absorption spectra on the nanosecond time scale were recorded on a custom-built pump-probe transient absorption setup. A 10 Hz Nd:YAG laser (Continuum Surelite) with a 5 ns pulse width was used to pump the excited state. The fundamental (1064 nm) passes a second-harmonic generation step (532 nm) followed by a third-harmonic generation to gain the frequency-tripled wavelength (355 nm). The beam is transmitted to an optical parametric oscillator (Continuum Surelite) generating tuneable wavelengths from 400 nm to 650 nm with energies ranging from 15 mJ to 80 mJ. If not stated otherwise an excitation wavelength of 440 nm and 20 mJ pulse energy was used. To record the ground state's transmission and probe the excited state, a 75 W xenon arc lamp (pulsed or CW) was used. Focusing the beam path with a concave mirror onto the sample the transmitted light is spectrally dispersed (Acton Princeton Instrument 2300), detected by a photomultiplier tube (Hamamatsu R928) and processed (Pascher Instruments AB).

Light-Driven Hydrogen Evolution Reactions

All photocatalytic reactions were performed with a 3D printed photoreactor utilizing a 405 nm LED from LEDENGIN (LZ4-00UB0R).⁴⁶ Samples were prepared in LABSOLUTE clear glass screw neck vials (ND13) and screw seals (ND13, butyl red / PTFE grey) (total volume 5 mL) under a nitrogen atmosphere. PS-CAT and BIH were dissolved into NMP



and CH₃CN which were degassed by freeze-pump-thaw. Photocatalytically produced hydrogen was quantified by the GC-2030 (column: SH-Rt-Msieve 5A, detector: BID (Dielectric-Barrier Discharge Ionization Detector)).

General procedure for the preparation of thioketones derivatives

A magnetically stirred solution of corresponding ketone **4-6** (1.0 mmol) in 10 mL THF was heated to 65 °C, followed by the addition of Lawesson's reagent (0.6 mmol) in a single portion. The mixture was then heated for 4 hours under an inert nitrogen gas atmosphere. Subsequently, the solvent was removed under reduced pressure, and the residue was purified by column chromatography using a *n*-hexane:CH₂Cl₂ (7:3) eluent, yielding the desired thioketone **PS-Fc-1**, **PS-Fc-2**, and **PS-Ph** as dark violet solid.

Compound **PS-Fc-1**: (69% yield). ¹H-NMR (600 MHz, CD₂Cl₂): δ 7.81 (d, *J*_{H-H} = 3.6 Hz, 1H), 7.59 (d, *J*_{H-H} = 8.4 Hz, 2H), 7.32-7.30 (m, 5H), 7.15-7.04 (m, 8H), 5.14 (s, 2H), 4.78 (s, 2H), 4.24 (s, 5H). ¹³C{¹H}-NMR (150.9 MHz, CD₂Cl₂): δ 220.6, 154.3, 152.4, 148.8, 147.1, 129.8, 129.4, 126.7, 125.1, 123.8, 123.5, 122.4, 89.1, 73.5, 72.8, 72.0. DEI-MS: *m/z* = 556 [M+H]⁺. Anal. Calcd for C₃₃H₂₅FeNS₂: C, 71.35; H, 4.54; S, 11.54. Found C, 71.44; H, 4.68; S, 11.64.

Compound **PS-Fc-2**: (65% yield). ¹H-NMR (600 MHz, CD₂Cl₂): δ 7.76 (d, *J*_{H-H} = 3.6 Hz, 1H), 7.50 (d, *J*_{H-H} = 8.4 Hz, 2H), 7.38 (d, *J*_{H-H} = 4.2 Hz, 1H), 7.31-7.28 (m, 4H), 7.25 (d, *J*_{H-H} = 4.2 Hz, 1H), 7.21 (d, *J*_{H-H} = 4.2 Hz, 1H), 7.13-7.05 (m, 9H), 5.14 (t, *J*_{H-H} = 1.8 Hz), 4.79 (t, *J*_{H-H} = 2.1 Hz), 4.23 (s, 5H). ¹³C{¹H}-NMR (150.9 MHz, CD₂Cl₂): δ 220.2, 152.5, 147.9, 147.4, 147.3, 145.4, 135.0, 129.4, 129.3, 127.2, 126.7, 126.4, 124.8, 124.5, 123.4, 123.1, 89.1, 73.7, 72.9, 72.1. DEI-MS: *m/z* = 638 [M+H]⁺. Anal. Calcd for C₃₇H₂₇FeNS₃: C, 69.69; H, 4.27; S, 15.08. Found C, 69.81; H, 4.34; S, 15.22.

Compound **PS-Ph**: (79% yield). ¹H-NMR (600 MHz, CD₂Cl₂): δ 7.67 (d, *J*_{H-H} = 7.2 Hz, 2H), 7.53 (t, *J*_{H-H} = 7.2 Hz, 1H), 7.49 (d, *J*_{H-H} = 8.4 Hz, 2H), 7.43-7.41 (m, 3H), 7.31-7.28 (m, 5H), 7.25 (d, *J*_{H-H} = 4.2 Hz, 1H), 7.22 (d, *J*_{H-H} = 4.2 Hz, 1H), 7.12 (d, *J*_{H-H} = 7.8 Hz, 4H), 7.09 (t, *J*_{H-H} = 7.2 Hz, 1H), 7.05 (d, *J*_{H-H} = 8.4 Hz, 2H). ¹³C{¹H}-NMR (150.9 MHz, CD₂Cl₂): δ 220.58, 153.0, 151.4, 148.2, 147.2, 146.9, 134.6, 132.9, 130.9, 129.4, 128.5,



128.0, 127.6, 127.0, 126.5, 125.0, 124.9, 123.5, 122.9. DEI-MS: $m/z = 530$ $[M+H]^+$. Anal. Calcd for $C_{33}H_{23}NS_3$: C, 74.82; H, 4.38; S, 18.16. Found C, 74.98; H, 4.44; S, 18.07.

General procedure for the preparation of diiron complexes

A 100 mL Schlenk flask was loaded with $Fe_3(CO)_{12}$ (0.52 mmol) along with compounds **PS-Fc-1**, **PS-Fc-2**, and **PS-Ph** (0.47 mmol), followed by the addition of 30 mL of dry THF. The resulting green solution was refluxed for 2 hours under an inert nitrogen atmosphere, during which the color gradually changed to deep red. Afterward, the solvent was evaporated under vacuum, and the crude products were purified using silica column chromatography with *n*-hexane: CH_2Cl_2 (5:1) as the eluent. The target products **PS-Fc-CAT-1**, **PS-Fc-CAT-2**, and **PS-Ph-CAT** were obtained from the first red-orange fractions, while **PS-Fc-CAT-3** was isolated from the second green fraction.

Complex **PS-Fc-CAT-1**: (46% yield). 1H -NMR (400 MHz, CD_2Cl_2): δ 7.58 (s, 1H), 7.50 (d, $J_{H-H} = 8.8$ Hz, 2H), 7.30 (dd, $J_{H-H} = 8.4$ Hz, 7.6 Hz, 4H), 7.13-7.04 (m, 8H), 5.41 (s, 1H), 4.20 (s, 5H), 4.09 (m, 2H), 3.97 (m, 1H), 3.21 (m, 1H). $^{13}C\{^1H\}$ -NMR (100.6 MHz, CD_2Cl_2): δ 209.7, 209.6, 165.8, 149.6, 149.0, 147.1, 135.1, 129.4, 127.5, 126.1, 125.1, 123.7, 122.5, 114.4, 91.1, 69.4, 68.5, 67.6, 67.3, 65.9, 58.2. IR (ν_{CO}): 2068, 2027, 1987 cm^{-1} . DEI-MS: $m/z = 834$ $[M]^+$, 778 $[M-2CO]^+$. Anal. Calcd for $C_{39}H_{25}Fe_3NO_6S_2$: C, 56.08; H, 3.02; S, 7.68. Found C, 56.19; H, 3.15; S, 7.76.

Complex **PS-Fc-CAT-2**: (41% yield). 1H -NMR (600 MHz, CD_2Cl_2): δ 7.52 (s, 1H), 7.49 (d, $J_{H-H} = 9.0$ Hz, 2H), 7.31-7.27 (m, 5H), 7.21 (d, $J_{H-H} = 4.2$ Hz, 1H), 7.13-7.05 (m, 8H), 5.40 (s, 1H), 4.22 (s, 5H), 4.10 (s, 2H), 3.99 (s, 1H), 3.26 (s, 1H). $^{13}C\{^1H\}$ -NMR (150.9 MHz, CD_2Cl_2): δ 209.6, 209.4, 165.8, 148.0, 147.3, 145.8, 142.7, 135.7, 133.6, 129.4, 127.1, 126.5, 124.8, 123.4, 123.0, 113.3, 90.9, 69.4, 68.6, 67.6, 67.4, 65.9, 58.2. IR (ν_{CO}): 2068, 2029, 1990 cm^{-1} . DEI-MS: $m/z = 918$ $[M+H]^+$. Anal. Calcd for $C_{43}H_{27}Fe_3NO_6S_3$: C, 56.30; H, 2.97; S, 10.48. Found C, 56.44; H, 3.05; S, 10.62.

Complex **PS-Fc-CAT-3**: (27% yield). 1H -NMR (600 MHz, CD_2Cl_2): δ 8.55 (d, $J_{H-H} = 10.2$ Hz, 1H), 7.97 (d, $J_{H-H} = 10.2$ Hz, 1H), 7.57-7.54 (m, 3H), 7.31 (t, $J_{H-H} = 7.8$ Hz, 5H), 7.26 (d, $J_{H-H} = 10.2$ Hz, 1H), 7.14-7.09 (m, 6H), 7.04 (d, $J_{H-H} = 9.0$ Hz, 1H), 4.74 (s, 1H), 4.44 (d, $J_{H-H} = 6.6$ Hz, 2H), 4.39 (s, 1H), 4.29 (s, 5H). $^{13}C\{^1H\}$ -NMR (150.9 MHz, CD_2Cl_2):



8213.6, 211.5, 209.1, 178.5, 151.9, 149.7, 148.6, 147.1, 140.0, 138.0, 129.4, 128.2, 126.8, 126.5, 125.2, 125.1, 123.8, 123.7, 122.5, 113.1, 84.5, 70.7, 69.9, 69.4, 68.8, 68.6, 66.0. IR (ν_{CO}): 2043, 2035, 2000, 1946 cm^{-1} . DEI-MS: $m/z = 918$ $[\text{M}]^+$, 890 $[\text{M-CO}]^+$, 862 $[\text{M-2CO}]^+$, 834 $[\text{M-3CO}]^+$, 806 $[\text{M-4CO}]^+$, 778 $[\text{M-5CO}]^+$. Anal. Calcd for $\text{C}_{43}\text{H}_{28}\text{Fe}_3\text{NO}_6\text{S}_3$: C, 56.23; H, 3.07; S, 10.47. Found C, 56.35; H, 3.18; S, 10.53.

Complex **PS-Ph-CAT**: (38% yield). $^1\text{H-NMR}$ (400 MHz, CD_2Cl_2): δ 7.64 (s, 1H), 7.48 (d, $J_{\text{H-H}} = 8.8$ Hz, 2H), 7.29 (t, $J_{\text{H-H}} = 7.8$ Hz, 4H), 7.22-7.17 (m, 5H), 7.12-7.03 (m, 8H), 6.60 (dd, $J_{\text{H-H}} = 2.8, 6.4$ Hz, 2H), 5.57 (s, 1H). $^{13}\text{C}\{^1\text{H}\}\text{-NMR}$ (100.6 MHz, CD_2Cl_2): δ 209.4, 209.2, 168.8, 148.0, 147.3, 146.1, 141.9, 135.6, 129.4, 128.3, 128.1, 127.7, 127.0, 126.5, 126.2, 124.8, 123.5, 123.0, 110.8, 60.06. APCI-MS (negative mode): $m/z = 724$ $[\text{M-3CO}]^-$, 640 $[\text{M-6CO}]^-$. Anal. Calcd for $\text{C}_{39}\text{H}_{23}\text{Fe}_2\text{NO}_6\text{S}_3$: C, 57.87; H, 2.86; S, 11.88. Found C, 57.95; H, 2.92; S, 11.82.

Conflicts of interest

There are no conflicts of interest to declare.

Acknowledgement

I. B. is thankful for the Deutsche Akademischer Austauschdienst (DAAD) for a scholarship. M. W. acknowledges Deutsche Forschungsgemeinschaft (German Research Foundation) via the TRR234 CATALIGHT, Projektnummer 364549901 (TP: Z2). We thank Dr. Stephan Kupfer (Uni Jena) for the fruitful discussions on the theory approaches and Prof. Christoph van Wüllen (RPTU) for the support in using the computation resources at RPTU. H.A.-F. acknowledges the financial support provided by the deanship of Scientific Research at the Hashemite University (38/2024).

References

- 1 D. G. Nocera, Solar Fuels and Solar Chemicals Industry, *Acc. Chem. Res.*, 2017, **50**, 616-619.
- 2 N. S. Lewis, Aspects of Science and Technology in Support of Legal and Policy Frameworks Associated with a Global Carbon Emissions-Control Regime, *Energy Environ. Sci.*, 2016, **6**, 2172-2176.



- 3 H. B. Gray, Powering the Planet with Solar Fuel, *Nat. Chem.*, 2009, **1**, 7.
- 4 H. Ishaq, I. Dincer, and C. Crawford, A Review on Hydrogen Production and Utilization: Challenges and Opportunities, *Int. J. Hydrog. Energy*, 2022, **47**, 26238-26264.
- 5 L.-Z. Wu, B. Chen, Z.-J. Li, and C.-H. Tung, Enhancement of the Efficiency of Photocatalytic Reduction of Protons to Hydrogen via Molecular Assembly, *Acc. Chem. Res.*, 2014, **47**, 2177-2185.
- 6 Z. Han, L. Shen, W. W. Brennessel, P. L. Holland, and R. Eisenberg, Nickel Pyridinethiolate Complexes as Catalysts for the Light-Driven Production of Hydrogen from Aqueous Solutions in Noble-Metal-Free Systems, *J. Am. Chem. Soc.*, 2013, **135**, 14659–14669.
- 7 L. Duan, F. Bozoglian, S. Mandal, B. Stewart, T. Privalov, A. Llobet, and L. Sun, A Molecular Ruthenium Catalyst with Water-Oxidation Activity Comparable to that of Photosystem II, *Nat. Chem.*, 2012, **4**, 418–423.
- 8 Y. Halpin, M. T. Pryce, S. Rau, D. Dini, and J. G. Vos, Recent Progress in the Development of Bimetallic Photocatalysts for Hydrogen Generation, *Dalton Trans.*, 2013, **42**, 16243-16254.
- 9 P. D. Frischmann, K. Mahata and F. Wurthel, Powering the Future of Molecular Artificial Photosynthesis with Light-Harvesting Metallosupramolecular Dye Assemblies, *Chem. Soc. Rev.*, 2013, **42**, 1847-1870.
- 10 W. T. Eckenhoff and R. Eisenberg, Molecular Systems for Light Driven Hydrogen Production, *Dalton Trans.*, 2012, **41**, 13004-13021.
- 11 M. Schulz, M. Karnahl, M. Schwalbe and J. G. Vos, The Role of the Bridging Ligand in Photocatalytic Supramolecular Assemblies for the Reduction of Protons and Carbon Dioxide, *Coord. Chem. Rev.*, 2012, **256**, 1682-1705.
- 12 W. Lubitz, H. Ogata, O. Rüdiger, and E. Reijerse, Hydrogenases, *Chem. Rev.*, 2014, **114**, 4081–4148.
- 13 M. W. Adams, The Structure and Mechanism of Iron-hydrogenases, *Biochim. Biophys. Acta*, 1990, **1020**, 115–145.
- 14 M. Frey, Hydrogenases: Hydrogen-Activating Enzymes, *ChemBioChem*, 2002, **3**, 153–160.



- 15 J. W. Peters, W. N. Lanzilotta, B. J. Lemon, and L. C. Seefeldt, X-ray Crystal Structure of the Fe-Only Hydrogenase (CpI) from *Clostridium pasteurianum* to 1.8 Angstrom Resolution, *Science*, 1998, **282**, 1853–1858.
- 16 A. Adamska, S. Roy, J. F. Siebel, T. R. Simmons, M. Fontecave, V. Artero, E. Reijerse, and W. Lubitz, Spectroscopic Characterization of the Bridging Amine in the Active Site of [FeFe] Hydrogenase Using Isotopologues of the H-cluster, *J. Am. Chem. Soc.*, 2015, **137**, 12744–12747 9.
- 17 H.-J. Fan, and M. B. Hall, A Capable Bridging Ligand for Fe-only Hydrogenase: Density Functional Calculations of a Low-Energy Route for Heterolytic Cleavage and Formation of Dihydrogen, *J. Am. Chem. Soc.*, 2001, **123**, 3828–3829.
- 18 L. R. Almazahreh, F. Arrigoni, H. Abul-Futouh, M. El-khateeb, H. Görls, C. Elleouet, P. Schollhammer, L. Bertini, L. De Gioia, M. Rudolph, G. Zampella, and W. Weigand, Proton Shuttle Mediated by (SCH₂)₂P=O Moiety in [FeFe]-Hydrogenase Mimics: Electrochemical and DFT Studies, *ACS Catal.*, 2021, **11**, 7080-7098.
- 19 H. Abul-Futouh, D. Costabel, K. Hotzel, P. Liebing, H. Görls, W. Weigand, and K. Peneva, Mono- and Di-Substituted [FeFe]-Hydrogenase H-cluster Mimics Bearing the 3,4-dimercaptobenzaldehyde Bridge Moiety: Insight into Synthesis, Characterization and Electrochemical Investigations, *Inorg. Chim. Acta*, 2023, **551**, 121469.
- 20 S. Gao, W. Fan, Y. Liu, D. Jiang, and Q. Duan, Artificial Water-Soluble Systems Inspired by [FeFe]-Hydrogenases for Electro- and Photocatalytic Hydrogen Production. *Int. J. Hydrogen Energy*, 2020, **45**, 4305–4327.
- 21 S. Gao, Y. Liu, Y. Shao, D. Jiang, and Q. Duan, Iron Carbonyl Compounds with Aromatic Dithiolate Bridges as Organometallic Mimics of [FeFe] Hydrogenases, *Coord. Chem. Rev.*, 2020, **402**, 213081, and references cited therein.
- 22 Y. Li, and T. B. Rauchfuss, Synthesis of Diiron(i) Dithiolato Carbonyl Complexes, *Chem. Rev.*, 2016, **116**, 7043–7077, and references cited therein.
- 23 H. Abul-Futouh, L. R. Almazahreh, S. J. Abaalkhail, H. Görls, S. T. Stripp, and W. Weigand, Ligand Effects on Structural, Protophilic and Reductive Features of Stannylated Dinuclear Iron Dithiolato Complexes, *New J. Chem.*, 2021, **45**, 36–44.



- 24 I. Basma, H. Abul-Futouh, S. J. Abaalkhail, P. Liebing, and W. Weigand, [FeFe]-Hydrogenase H-Cluster Mimics Mediated by Ferrocenyl Hetaryl Thioketone Derivatives, *J. Mol. Struct.*, 2024, **1295**, 136630.
- 25 Z.-Y. Ma, X.-F. Liu, B. Jin, D. Wang, and P.-H. Zhao, Substituent Effects of Tertiary Phosphines on the Structures and Electrochemical Performances of Azadithiolato-Bridged Diiron Model Complexes of [FeFe]-Hydrogenases, *Appl. Organomet. Chem.*, 2022, **36**, e6751.
- 26 T. Yu, Y. Zeng, J. Chen, Y.-Y. Li, G. Yang, and Y. Li, Exceptional Dendrimer-Based Mimics of Diiron Hydrogenase for the Photo-chemical Production of Hydrogen, *Angew. Chem., Int. Ed.*, 2013, **52**, 5631–5635.
- 27 K. A. Brown, M. B. Wilker, M. Boehm, G. Dukovic, and P. W. King, Characterization of Photochemical Processes for H₂ Production by CdS Nanorod-[FeFe] Hydrogenase Complexes, *J. Am. Chem. Soc.*, 2012, **134**, 5627–5636.
- 28 W.-G. Wang, F. Wang, H.-Y. Wang, G. Si, C.-H. Tung, and L.-Z. Wu, Photocatalytic Hydrogen Evolution by [FeFe] Hydrogenase Mimics in Homogeneous Solution., *Chem. Asian J.*, 2010, **5**, 1796–1803.
- 29 F. Wang, W.-G. Wang, H.-Y. Wang, G. Si, C.-H. Tung, and L.-Z. Wu, Artificial Photosynthetic Systems Based on [FeFe]-Hydrogenase Mimics: The Road to High Efficiency for Light-Driven Hydrogen Evolution. *ACS Catal.*, 2012, **2**, 407–416.
- 30 S. Fukuzumi, Y. Lee, and W. Nam, Thermal and Photocatalytic Production of Hydrogen with Earth-Abundant Metal Complexes, *Coord. Chem. Rev.*, 2018, **355**, 54–73.
- 31 J. Amaro-Gahete, M. V. Pavliuk, H. Tian, D. Esquivel, F. J. Romero-Salguero, and S. Ott, Catalytic Systems Mimicking the [FeFe]-Hydrogenase Active Site for Visible-Light-Driven Hydrogen Production, *Coord. Chem. Rev.*, 2021, **448**, 214172.
- 32 S. Ott, M. Kritikos, B. Åkermark, and L. Sun, Synthesis and structure of a biomimetic model of the iron hydrogenase active site covalently linked to a ruthenium photosensitizer, *Angew. Chem. Int. Ed.*, 2003, **42**, 3285–3288.



- 33 X. Li, M. Wang, S. Zhang, J. Pan, Y. Na, J. Liu, B. Åkermark, and L. Sun, Noncovalent assembly of a metalloporphyrin and an iron hydrogenase active-site model: photo-induced electron transfer and hydrogen generation, *J. Phys. Chem. B*, 2008, **112**, 8198–8202.
- 34 L.-C. Song, M.-Y. Tang, F.-H. Su, and Q.-M. Hu, A Biomimetic model for the active site of iron-only hydrogenases covalently bonded to a porphyrin photosensitizer, *Angew. Chem. Int. Ed.*, 2006, **45**, 1130–1133.
- 35 L.-C. Song, L.-X. Wang, M.-Y. Tang, C.-G. Li, H.-B. Song, Q.-M. Hu, Synthesis, structure, and photoinduced catalysis of [FeFe]-hydrogenase active site models covalently linked to a porphyrin or metalloporphyrin moiety, *Organometallics*, 2009, **28**, 3834–3841.
- 36 A. P. S. Samuel, D. T. Co, C. L. Stern, and M. R. Wasielewski, Ultrafast photodriven intramolecular electron transfer from a zinc porphyrin to a readily reduced diiron hydrogenase model complex, *J. Am. Chem. Soc.*, 2010, **132**, 8813–8815.
- 37 L. Sun, B. Åkermark, and S. Ott, Iron hydrogenase active site mimics in supramolecular systems aiming for light-driven hydrogen production, *Coord. Chem. Rev.*, 2005, **249**, 1653–1663.
- 38 J. Ekström, M. Abrahamsson, C. Olson, J. Bergquist, F. B. Kaynak, L. Eriksson, L. Sun, H.-C. Becker, B. Åkermark, L. Hammarström, and S. Ott, Bio-inspired, side-on attachment of a ruthenium photosensitizer to an iron hydrogenase active site model, *Dalton Trans.*, 2006, 4599–4606.
- 39 W. Gao, J. Liu, W. Jiang, M. Wang, L. Weng, B. Åkermark, and L. Sun, An azadithiolate bridged Fe₂S₂ complex as active site model of FeFe hydrogenase covalently linked to a Re(CO)₃(bpy)(py) photosensitizer aiming for light-driven hydrogen production, *Comptes Rendus Chim.*, 2008, **11**, 915–921.
- 40 A. M. Kluwer, R. Kapre, F. Hartl, M. Lutz, A. L. Spek, A. M. Brouwer, P. W. N. M. van Leeuwen, and J. N. H. Reek, Self-assembled biomimetic [2Fe₂S]-hydrogenase based photocatalyst for molecular hydrogen evolution, *Proc. Natl. Acad. Sci. (U.S.A.)*, 2009, **106**, 10460–10465.



- 41 H.-H. Cui, M.-Q. Hu, H.-M. Wen, G.-L. Chai, C.-B. Ma, H. Chen, and C.-N. Chen, Efficient [FeFe] hydrogenase mimic dyads covalently linking to iridium photosensitizer for photocatalytic hydrogen evolution, *Dalton Trans.*, 2012, **41**, 13899-13907.
- 42 S. Ott, M. Borgström, M. Kritikos, R. Lomoth, J. Bergquist, B. Åkermark, L. Hammarström, and L. Sun, Model of the iron hydrogenase active site covalently linked to a ruthenium photosensitizer: synthesis and photophysical properties, *Inorg. Chem.*, 2004, **43**, 4683–4692.
- 43 S. Gao, W.-Y. Zhang, Q. Duan, Q.-C. Liang, D.-Y. Jiang, J.-X. Zhao, and J.-H. Hou, An artificial [FeFe]-hydrogenase mimic with organic chromophore-linked thiolate bridges for the photochemical production of hydrogen, *Chem. Pap.*, 2017, **71**, 617–625.
- 44 R. Goy, U.-P. Apfel, C. Elleouet, D. Escudero, M. Elstner, H. Görls, J. Talarmin, P. Schollhammer, L. González, and W. Weigand, A Silicon-heteroaromatic system as photosensitizer for light-driven hydrogen production by hydrogenase mimics, *Eur. J. Inorg. Chem.*, 2013, 4466–4472.
- 45 R. Goy, L. Bertini, T. Rudolph, S. Lin, M. Schulz, G. Zampella, B. Dietzek, F. H. Schacher, L. De Gioia, K. Sakai, and W. Weigand, Photocatalytic hydrogen evolution driven by [FeFe] hydrogenase models tethered to fluorene and silafluorene sensitizers, *Chem. Eur. J.*, 2017, **23**, 334–345.
- 46 P. Buday, C. Kasahara, E. Hofmeister, D. Kowalczyk, M. K. Farh, S. Riediger, M. Schulz, M. Wächter, S. Furukawa, M. Saito, D. Ziegenbalg, S. Gräfe, P. Bäuerle, S. Kupfer, B. Dietzek-Ivanšić, and W. Weigand, Activating a [FeFe] Hydrogenase Mimic for Hydrogen Evolution under Visible Light, *Angew. Chem. Int. Ed.*, 2022, **61**, e202202079.
- 47 A. Q. Daraosheh, H. Abul-Futouh, N. Murakami, K. M. Ziems, H. Görls, S. Kupfer, S. Gräfe, A. Ishii, M. Celeda, G. Mloston, and W. Weigand, Novel [FeFe]-Hydrogenase Mimics: Unexpected Course of the Reaction of Ferrocenyl α -Thienyl Thioketone with $\text{Fe}_3(\text{CO})_{12}$, *Materials*, 2022, **15**, 2867.
- 48 I. Basma, S. J. Abaalkhail, H. Abul-Futouh, P. Liebing, P. Matczak, G. Mloston, and W. Weigand, Trophothione as a remarkable 8π electron substrate in



- complexation reaction with $\text{Fe}_3(\text{CO})_{12}$: Experimental and computational studies, *Inorg. Chem. Commun.*, 2025, **174**, 114025.
- 49 X. Wu, W. Wu, C. Cui, J. Zhao, and M. Wu, Preparation of Bodipy–ferrocene dyads and modulation of the singlet/triplet excited state of bodipy via electron transfer and triplet energy transfer, *J. Mater. Chem. C*, 2016, **4**, 2843-2853.
- 50 M. Supur, M. E. El-khouly, J. H. Seok, J. H. Kim, K.-Y. Kay, and S. Fukuzumi, Efficient Electron Transfer Processes of the Covalently Linked Perylenediimide–Ferrocene Systems: Femtosecond and Nanosecond Transient Absorption Studies, *J. Phys. Chem. C*, 2010, **114**, 10969-10977.
- 51 D. M. S. C. Dissanayake, M. H. Dinh, J. J. Kuchta, and A. K. Vannucci, Ferrocene-Mediated Photochemical Reduction of Naphthol to Generate Hydrogen, *Chem. Eur. J.*, 2025, e01540.
- 52 R. Itagki, S.-Y. Takizawa, H.-C. Chang, and A. Nakada, Light-induced electron transfer/phase migration of a redox mediator for photocatalytic C–C coupling in a biphasic solution, *Dalton Trans.*, 2022, **51**, 9467-9476.
- 53 E. Maligaspe, M. R. Hauwiller, Y. V. Zatsikha, J. A. Hinke, P. V. Solntsev, D. A. Blank, and V. N. Nemykin, Redox and Photoinduced Electron-Transfer Properties in Short Distance Organoboryl Ferrocene-Subphthalocyanine Dyads, *Inorg. Chem.*, 2014, **53**, 9336-9347.
- 54 H. Miyake, T. Tajima, and Y. Takaguchi, Synthesis and Light-absorption Characteristics of Thiophene Derivatives Bearing Ferrocenylthiocarbonyl Groups, *Chem. Lett.*, 2017, **46**, 48-50.
- 55 P. Kumaresan, Y.-Y. Liu, S. Vegiraju, Y. Ezhumalai, H.-C. Yu, S. L. Yau, M.-C. Chen, and T.-C. Lin, Synthesis and Characterization of Two-Photon Active Chromophores Based on Tetrathienoacene (TTA) and Dithienothiophene (DTT), *Chem. Asian J.*, 2015, **10**, 1640-1646.
- 56 Y. Li, J. Hu, G. He, H. Zhu, X. Wang, Q. Guo, A. Xia, Y. Lin, J. Wang, and X. Zhan, Influence of Thiophene Moiety on the Excited State Properties of Push–Pull Chromophores, *J. Phys. Chem. C*, 2016, **120**, 26 (13922-13930).
- 57 S. Roquet, A. Cravino, P. Leriche, O. Alévêque, P. Frère, and J. Roncali, Triphenylamine–thienylenevinylene hybrid systems with internal charge transfer



- as donor materials for heterojunction solar cells, *J. Am. Chem. Soc.*, 2006, **128**, 3459-3466.
- 58 H. Kanato, K. Takimiya, T. Otsubo, Y. Aso, T. Nakamura, Y. Araki, and O. Ito, Synthesis and photophysical properties of ferrocene-oligothiophene-fullerene triads, *J. Org. Chem.*, 2004, **69**, 7183–7189.
- 59 X. Wu, W. Wu, X. Cui, J. Zhao, and M. Wu, Preparation of Bodipy-ferrocene dyads and modulation of the singlet/triplet excited state of bodipy via electron transfer and triplet energy transfer, *J. Mater. Chem. C*, 2016, **4**, 2843-2853.
- 60 H. Wang, G. Si, W. Cao, W. Wang, Z. Li, F. Wang, C. Tung, and L. Wu, A triad [FeFe] hydrogenase system for light-driven hydrogen evolution, *Chem. Commun.*, 2011, **47**, 8406-8408.
- 61 R. Giasson, E. J. Lee, X. Zhao, and M. S. Wrighton, Inter-and intramolecular quenching of the singlet excited state of porphyrins by ferrocene, *J. Phys. Chem.*, 1993, **97**, 2596-2601.
- 62 C. Kasahara, K. Rediger, M. Micheel, P. Liebing, S. Gräfe, S. Kupfer, M. Wächter, and W. Weigand, Molecular Dyad vs Multi-Component Approach-Photocatalytic Hydrogen Evolution by Combining Oligothiophene Photosensitizers with [FeFe]-Hydrogenase Mimics, *ChemCatChem*, 2024, **16**, e202400247.
- 63 A. Farmilo, and F. Wilkinson, Triplet state quenching by ferrocene, *Chem. Phys. Lett.*, 1975, **34**, 575-580.
- 64 G. Mlostoń, R. Hamera, and H. Heimgartner, Synthesis of Ferrocenyl Thioketones and their Reactions with Diphenyldiazomethane, *Phosphorus, Sulfur, and Silicon and Rel. Elem.*, 2015, **190**, 2125–2133.
- 65 J. Skiba, R. Karpowicz, I. Szabó, B. Therrien, and K. Kowalski. Synthesis and anticancer activity studies of ferrocenyl-thymine-3,6-dihydro-2H-thiopyranes - A new class of metallocene-nucleobase derivatives, *J. Organometal. Chem.*, 2015, **794**, 216–222.
- 66 G. Mlostoń, R. Hamera-Fałdyga, M. Celeda, and H. Heimgartner, Efficient synthesis of ferrocifens and other ferrocenyl-substituted ethylenes *via* a ‘sulfur approach’, *Org. Biomol. Chem.*, 2018, **16**, 4350–4356.



- 67 G. Mlostoń, R. Hamera-Faldyga, K. Urbaniak, W. Weigand, and H. Heimgartner, A convenient access to 1,2-diferrocenyl-substituted ethylenes via [3 + 2]-cycloelimination of 2-silylated 4,4,5,5-tetrasubstituted 1,3-dithiolanes, *J. Sulfur Chem.*, 2018, **39**, 516–524.
- 68 N. Murakami, H. Miyake, T. Tajima, K. Nishikawa, R. Hirayama, and Y. Takaguchi, Enhanced Photosensitized Hydrogen Production by Encapsulation of Ferrocenyl Dyes into Single-Walled Carbon Nanotubes, *J. Am. Chem. Soc.*, 2018, **140**, 3821–3824.
- 69 G. M. Sheldrick, SHELXT-Integrated Space-Group and Crystal-Structure Determination, *Acta Crystallogr.*, 2015, **A71**, 3–8.
- 70 G. M. Sheldrick, Crystal Structure Refinement with SHELXL, *Acta Crystallogr.*, 2015, **C71**, 3–8.
- 71 O. V. Dolomanov, L. J. Bourhis, R. J. Gildea, J. A. K. Howard, and H. Puschmann, OLEX2: A Complete Structure Solution, Refinement and Analysis Program, *J. Appl. Crystallogr.*, 2009, **42**, 339–341.
- 72 Bruker AXS 2001, Apex4 and SADABS, Bruker AXS Inc., Madison, Wisconsin, USA.



Data Availability Statement

[View Article Online](#)
DOI: 10.1039/D5QI01191D

The data supporting this article have been included as part of the Supplementary Information

